High-performance phototransistors based on PDIF-CN_2 solution-processed single fiber and multi-fiber assembly

Wassima Rekab, Marc A. Stoeckel, Mirella El Gemayel, Marco Gobbi, Emanuele Orgiu and Paolo Samorì**

Nanochemistry Laboratory, ISIS & icFRC, Université de Strasbourg & CNRS,

8 allée Gaspard Monge, 67000 Strasbourg, France

*E-mail: samori@unistra.fr , orgiu@unistra.fr

KEYWORDS: perylene di-imide, organic field-effect transistor, photoconductivity, phototransistor, single fiber.

ABSTRACT:

Here we describe the fabrication of organic phototransistors based on either single or multi-fibers integrated in three-terminal devices. These self-assembled fibers have been produced by solvent-induced precipitation of an air stable and solution-processable perylene diimide derivative, i.e. PDIF-CN2. The opto-electronic properties of these devices were compared to devices incorporating more disordered spin-coated PDIF-CN2 thin-films. The single-fiber devices revealed significantly higher field-effect mobilities, compared to multifiber and thin-films, exceeding 2 $cm^2V^{-1}s^{-1}$. Such an efficient charge transport is the result of strong intermolecular coupling between closely packed PDIF-CN2 molecules and of a low density of structural defects. The improved crystallinity allows efficient collection of photogenerated Frenkel excitons which results in the highest reported responsivity (R) for single-fiber PDI-based phototransistors, and photosensitivity (P) exceeding 2×10^3 AW^{-1}, and 5×10^3, respectively. These findings provide unambiguous evidence for the key role played by the high degree of order at the supramolecular level to leverage the material's properties towards the fabrication of light-sensitive organic field-effect transistors combining a good operational stability, high responsivity and photosensitivity. Our results show also that the air-stability performances are superior in devices where highly crystalline supramolecularly engineered architectures serve as the active layer.

1. INTRODUCTION

The fabrication and optimization of organic field-effect transistors (OFETs) have been the subject of an intense research endeavor during the last decade because such devices represent key elements for low-cost flexible electronics including radiofrequency identification (RFID) tags,[1-7] integrated circuits (ICs) for logic and memory chips, smart cards and sensors.[8-14] Organic-based electronics can play an important role also in other applications including electronic bar codes or active matrix elements for displays,[15-16] light-emitting diodes,[17-18] and photovoltaics[19].

Organic phototransistors, i.e. OFETs in which an incident light is used in addition to a gate field to modulate the charge-carrier density inside the channel, have many advantages over their inorganic counterparts, such as the tunability of their optoelectronic properties via the molecular design and their possibility to be assembled on non-planar supports opening perspectives towards their flexible thus wearable applications.[20-29] Low-dimensional organic architectures such as crystalline micro/nanowire,[30-38] microribbon[39] and quantum dot[40-41] structures have showed high photosensitivity and high charge carrier properties. Among organic semiconducting molecules used as active components in efficient phototransistors, perylene di-imide (PDI) derivatives are particularly suitable because of their characteristic absorption in the visible region combined with the capacity to transport electrons.[42-53] One of the major limitations of organic transistors, especially those based on n-type systems, is their air sensitivity. To overcome such a limitation, we have focused our attention on air-stable *n*-type perylene di-imide derivative, i.e. N, N'-1H, 1H-perfluorobutyl-dicyano perylene diimide (PDIF-CN2) (**Figure 1**), which is known to form highly crystalline fibers by solvent-induced precipitation (SIP), being a simple solution-processable method to produce high-performing crystalline structures with respect to those that

are vapor-grown. Such self-assembled fibers exhibit a much higher degree of crystallinity when compared to spin-coated thin-films obtained from the same molecule (Figure S11). Selected-area electronic-diffraction (SAED) studies on PDIF-CN2 single fibers deposited on SiO_2 performed previously in our group[54] confirmed that molecules self-assemble in an edge-on orientation on the basal plane of the surface with the fluoroalkyl chains embedded in-between the aromatic cores and the SiO_2 dielectric. Different types of architectures based on PDIF-CN_2 have shown extremely high field-effect mobilities qualifying this system as reference n-type semiconductor for organic electronics.[55-60]

In this paper we report on the integration of various types of PDIF-CN_2 architectures, including single fibers, multiple fibers and spin-coated films, in three-terminal devices while evaluating the influence of the different interfaces, i.e. metal/semiconductor and dielectric/semiconductor, on the electrical performances. In addition, we have carried out an exhaustive study of the light responsive properties of these different PDIF-CN_2 architectures making it possible to elucidate the relationship between molecular order and photoresponsivity.

2. EXPERIMENTAL SECTION

PDIF-CN2 is dissolved in chloroform (99, 0-99, 4% GC) in a concentration of 2 mg/ml. The solutions are heated at 50°C until the molecules are completely dissolved. We have fabricated transistors in two configurations, i.e. bottom-contact-bottom-gate and top-contact-bottom-gate configuration. Highly doped n-type silicon wafers were used as substrate for the organic OFETs. The thermally-grown SiO_2 layers (230 nm) have a unit area capacitance (C_i) of 15 $nFcm^{-2}$. Micro-lithographed 40 nm thick gold source and drain electrodes were patterned on the dielectric substrate. SiO_2 substrates are protected by a photoresist layer that is washed off prior to use. The

substrates should be extremely pure since impurities can act as charge carrier traps; because of this reason they were cleaned with acetone (95% GC) and isopropanol (99.7 % GC) in an ultrasonic bath (20 minutes in each solvent) followed by a gentle drying under nitrogen gas. After that, the substrate surface was treated with UV/Ozone cleaning and functionalized with HMDS self-assembled monolayers by spin-coating 100 μl HMDS solutions (0.47 mM) onto the substrate surface for 60 seconds at 1500 rpm, followed by thermal annealing at 100 °C for 1 hour. Alternatively, octadecyltrichlorosilane (OTS) SAMs were grown: in this case the substrates were immersed into a 10 mM solution of OTS in anhydrous toluene and annealed at 60 °C for 30 minutes; after that, the substrates were left for 12 hours, washed with anhydrous toluene and dried in the spin-coater (4000 rpm, 60 seconds), and finally annealed at 60 °C for 1 hour. Afterwards, the Au source-drain electrode surface was functionalized with chemisorbed undecanethiol ($C_{11}H_{23}$-SH) SAMs. The presence of such SAM on Au surface lowers the metal work function by rendering it closer to the LUMO energy level of the PDIF-CN2 which amounts to -4.5 eV. OFET substrates were immersed in a 1 mM solution of undecanethiol in ethanol for 12 hours in order to enable the SAMs formation onto the electrodes. The substrates were then washed with copious amounts of absolute ethanol to remove the physisorbed undecanethiol molecules from the dielectric and electrode surfaces.[61] The PDIF-CN2 was spin-coated on the dielectric surfaces by applying a 100 μl drop of PDIF-CN2 solution in chloroform onto the substrate and spin it at 1500 RPM for 60 seconds inside the glove box. The device was then annealed at 60°C for 1 hour. On the other hand, in the SIP process, 150 μl of PDIF-CN2 solution in chloroform was injected rapidly in 950 μl of ethanol (CH_3OH, 99,9% GLC). Within a period of 15 minutes the fibers were formed in solution and precipitated on the bottom of vials. The

fibers were then transferred to the surface by dropping multiple times 20 μl until the full surface coverage was reached.

To improve the physical contact of multifiber assemblies with source and drain electrodes, we have also fabricated devices in top-contact configuration with the same gate insulator surface treatments (OTS self-assembled monolayers) used for bottom-contact devices. The fibers were deposited by SIP on SiO_2 surfaces, then we evaporated on the top source and drain gold electrodes through a shadow mask inside a vacuum chamber at pressure of 10^{-6} mbar. The evaporation rate was maintained at ~0.02-0.04 nm/s. In this way 50 nm thick films top Au electrodes were grown. The evaporation was done by using Plassys ME300B thermal evaporator.

Single-fiber devices were fabricated using a top-contact bottom-gate geometry. Before depositing the single fiber, the SiO_2 surface was functionalized with OTS to minimize interfacial trapping sites for charges during device operation. SIP fibers were cast onto the functionalized SiO_2 substrates followed by the deposition of 40-nm-thick Au electrodes by thermal evaporation.

The current-voltage (I-V) characteristics of all devices were measured inside the glove box in nitrogen atmosphere. The air-stability tests performed under illumination were carried out outside the glove box at controlled room temperature and humidity (T = 22 °C, RH% ~25) by contacting the source, drain and gate electrodes and applying different voltages using a Cascade Microtech M150 probe station with dual channel Keithley 2636A source-meter and associated software. Phototransistors devices were characterized in dark and under light irradiation from the top using a Leica LED1000 OLED ring (white light, 5.06 $mWcm^{-2}$) and an Optometric LLC TLS-25 M tunable light source with a monochromatic beam, light irradiation was performed at 525 nm wavelength at either 4.84 $mWcm^{-2}$ or 7.24 μWcm^{-2} light intensity.

The electron mobility was extracted in the saturation regime according to the equation:

$$\mu_{sat} = \frac{2 \cdot \left(\frac{\partial \sqrt{I_D}}{\partial V_{GS}} \right)^2}{C_i \frac{W}{L}}$$

where I_D is the current measured between source and drain electrodes, V_{GS} the potential difference measured between the voltage probes, L their distance, W the channel width and C_i the capacitance per unit area of the insulator layer.

3. RESULTS AND DISCUSSION

The development of high performance OFETs requires the electrodes to be bridged by highly crystalline semiconducting architectures forming continuous percolation pathways for the transport of charges. Transistors fabricated on untreated SiO_2 exhibited poor charge transport characteristics for both multifiber assemblies and spin-coated devices (see below). In order to promote the packing of spin-coated molecules while studying the assembly of the PDIF-CN2 fibers at the surface, the SiO_2 dielectric substrate was modified with UV-Ozone treatment and functionalized with either hexamethyldisilazane (HMDS) or octadecyltrichlorosilane (OTS) self-assembled monolayers. Moreover, the chemisorption of undecanethiols ($C_{11}H_{23}$-SH) on Au electrodes guaranteed simultaneously an improved hydrophobic nature of the metallic surface to promote physisorption of the organic semiconductor, thus ensuring a good physical contact, and an optimization of the injection of charges from the electrodes into the LUMO of the semiconductor by decreasing the Au electrode work function of ca. 250 meV.

Table 1 summarizes the different field-effect mobility values extracted from saturation regime as well as threshold voltage (V_{th}) for bottom-contact bottom-gate devices based on multi-

fiber structures. It reveals that the best mobilities are measured on OFET devices which underwent OTS or HMDS treatment followed by chemisorption of undecanethiol SAMs on the Au electrodes. Noteworthy, our results show that the charge injection from the functionalized gold electrodes leads to negligible enhancements in both mobility and V_{th}. The devices with untreated SiO_2 displayed very low mobility values on the order of 10^{-6} $cm^2V^{-1}s^{-1}$ for both multifiber and spin-coated devices. Ideally, the dielectric surface should provide a favorable environment to allow the generation of π-π stacked architectures in order to form highly ordered organic films. The chemisorption of hydrophobic SAMs on SiO_2 reduces the surface energy of SiO_2 while decreasing the trapping induced by the Si–OH groups, giving a more favorable environment for the organic semiconductor molecules deposition, especially for spin-coated films[62]. We recorded a significant improvement in the curve shape, yield of working devices as well as mobility (on the order of 10^{-3} $cm^2V^{-1}s^{-1}$) and threshold voltage when the SiO_2 was treated with OTS or HMDS which ensured reduced inter-fiber aggregation and a better interface with the dielectric surface (see **Figure 2**).

Figure 3 portrays the output and transfer curves of PDIF-CN2 spin-coated thin-films, multi- and single-fiber devices. Single-fibers based FET revealed mobility values as high as 2.3 $cm^2V^{-1}s^{-1}$ (average mobility 0.9 $cm^2V^{-1}s^{-1}$) and low threshold voltage values around -10 V for single-fiber FET as reported in **Table 2** and **Figure 4**. Such performances provide unambiguous evidence for an enhanced charge transport through crystalline fibers, albeit non-uniform, [63] when compared to the amorphous spin-coated films (annealed at 60 °C for 1 hour) which featured an average mobility of 2.8×10^{-2} $cm^2V^{-1}s^{-1}$. On the other hand, multifiber FETs displayed field-effect mobilities of ca. 3.8×10^{-3} $cm^2V^{-1}s^{-1}$, thus being nearly three orders of magnitude lower than those measured in single-fiber FETs. Such a discrepancy can be explained by considering

the fiber-to-fiber grain boundaries: in multifiber assemblies, charge carriers may hop from one fiber to the neighboring one(s) in order to be collected at the electrode; this process strongly limits the transport. This observation has been confirmed by probing the electron charge transport between two different interconnected fibers as displayed in **Figure S1a**. The field-effect mobility in the saturation region (see the corresponding output-curve in **Figure S1c**), is ~1.7×10^{-3} $cm^2V^{-1}s^{-1}$ which compares well with those extracted from multifiber devices. To further explain such low mobility, we investigated the charge transport through crossing (and therefore overlapping) fibers (see **Figure S1b** and **S1d**). This exemplary experiment revealed that in some cases the gate effect in the device can be negligible. Such a behavior can be ascribed to a low and ineffective electrostatic coupling owing to the presence of (two or more) fibers sitting underneath the measured fiber (the one connected to Au gold electrodes) which separate it from the gate electric field.

In addition, the effect of a mild thermal annealing was tested on both thin-film and multifiber FETs in order to improve the degree of crystallinity within the sample. For spin-coated devices, annealing at 60 °C for 1 hour led to an increase in their electrical performances as shown in **Table S1.**

With the aim of gaining greater insight into the charge injection at the electrode/semiconductor interface in multifiber-based devices, the top-contact configuration was implemented by thermally evaporating Au source and drain electrodes on pre-assembled fibers physisorbed on a treated SiO_2 surface (top-contact bottom-gate configuration). Unfortunately, the use of top electrodes does not allow the electrode functionalization with thiolated molecules, to guarantee optimal metal/semiconductor interface energetics. The deposition of gold electrodes on the top of the fibers led to non-functioning devices (see **Figure S2)** owing to an uneven and

not continuous top gold layer connecting the fibers (fibers' average thickness being within few hundreds of nm). Unfortunately, the scenario was unchanged even upon evaporation of gold layers with a thickness up to 150 nm (see **Figure S3**).

Figure S4 shows different assembly of fibers on treated and untreated SiO_2 surface. It reveals a propensity to form single layers of fibers on SiO_2 surfaces treated with OTS and HMDS. Morphological and charge transport characterization demonstrated that the hydrophobic nature of the substrate surface has a major impact on the final response of the devices. In order to verify both reliability and reproducibility of the OFET devices based on multifiber assemblies a large number of devices (>100) were prepared on both HMDS-/OTS-treated and untreated silicon dioxide substrates. All fabricated OFETs exhibit the same performances, proving a good reproducibility of the Solvent Induced Precipitation process used to make them.

The light responsive nature of the electrical characteristics of multifiber-based assemblies compared with those of thin-film and single-fiber devices were quantified by determining the photoresponsivity R and the photoswitching ratio, i.e. photosensitivity, P (photocurrent/dark-current) of the devices. This has been accomplished by measuring the I-V characteristics of the transistors under white and monochromatic light irradiation. The R and P values are defined as:

$$R = \frac{(I_{light} - I_{dark})}{EWL}$$

$$P = \frac{(I_{light} - I_{dark})}{I_{dark}}$$

Where W and L are the channel width and length, E is the incident illumination power (areal) density on the channel of the device, I_{light} the drain current under illumination, and I_{dark} the drain

current measured in dark conditions. The *R* and *P* values were plotted as a function of V_G for the thin-film, single fiber and multifiber-based devices.

Figure 5 displays the difference in transfer and output characteristics for (a, b) multifiber-based OPTs, (c,d) thin-film OPTs, and (e,f) single-fiber OPTs in dark and under illumination with white light ($\lambda > 400$ nm, 5.06 $mWcm^{-2}$). It reveals a general increase of the drain current in the I_{DS}-V_{DS} and I_{DS}-V_G curves upon irradiation as a result of photogenerated charge carriers. In particular, under light irradiation, the *off*-current of the single-fiber OPT, multifiber OPT and thin-film OPT were significantly higher indicating that the minimum conductivity measurable in the film (σ_{min}) increased owing to the additional contribution of photogenerated charges. In addition, the threshold voltage (V_{th}) shifted towards more negative voltages (n-doping), implying the easier turn-on of the device. This could be ascribed to the more efficient filling of trap sites by the photogenerated extra charge component.

Light responsivity (R) and photocurrent/dark-current ratio (P) are important parameters for investigating the capacity of a material to respond to light stimuli. **Figure 6** shows that when illuminated with white light the multifiber OPTs exhibit a maximum R value of 200 AW^{-1} with a corresponding P = 3.3, whereas thin-film-OPTs display R_{max} = 24 AW^{-1} and P_{max} = 0.6 (these values were reported from devices with the same channel length for both thin-film and multifiber OPTs). For single-fiber OPTs devices, a maximum R value of 2189 AW^{-1} at a gate voltage of 60 V with a corresponding P value of 5001 were recorded under white light irradiation. In **Figure S5**, the same single-fiber OPT device (in **Figure 6**) was also irradiated using green light (4.84 $mWcm^{-2}$). The calculated R and P values were comparable to those obtained under white light irradiation, amounting ca. to 2593 AW^{-1} and 4560, respectively.

Under white light illumination all investigated PDI-based single-fiber OPTs exhibited responsivity and photoswitching ratio both exceeding 10^3 indicating a pronounced increase of the signal upon irradiation. The multifiber OPTs exhibited responsivity being lower than that of single-fiber OPTs yet one order of magnitude higher compared to those of thin-film based-OPTs. The increase in R in the case of single fibers compared to the thin-film devices can be ascribed to the improved molecular order within the fibers which enables a better transport of the photogenerated carriers to the electrodes. Conversely, the diffusion of the generated Frenkel excitons towards the electrodes is more impeded in the multifiber devices compared to that in single-fiber devices owing to the energetically unfavored fiber-to-fiber energy transfer. The hopping mechanism of excitons in organic semiconductors is generally considered to be a dipole-dipole resonance energy transfer known as the Förster mechanism[64-65]. Such mechanism is based on short-range interactions which vanish as $1/d^6$ where d is the distance between the molecular entities. In our case, the intermolecular π-π distance is ca. 3.3 Å which is far shorter than two fluorinated alkyl chains in a row. Hence, we ascribe the poor photoresponse of multifiber devices to the poor fiber-to-fiber exciton transport.

Significantly, the photoresponsivity R and photocurrent/dark current ratio P values that we obtained in the present study concerning single-fiber OPTs are, to the best of our knowledge, the highest reported in literature for perylene di-imide single crystal-based organic phototransistors.[48-50] For instance, the maximum R reported for BPE-PTCDI NW-OPTs, amounts to ca. 1400 AW^{-1} at a gate voltage of 100 V and photoswitching current of 4960 for top-contact devices irradiated with green light, corresponding to a darkness charge carrier mobility of 1.13 $cm^2V^{-1}s^{-1}$.[50] The photoresponsivity of PTCDI-C_8 (perylene derivative) single nanowires-OPTs was about 7 AW^{-1}.[49] Yu et al. demonstrated that the light response increased by increasing the

charge carrier mobility devices,[50] which was observed in previous reports on organic phototransistors[32, 35, 39] and confirmed in our case, where the highest R was obtained from OFET device exhibiting high charge mobility (2.3 $cm^2V^{-1}s^{-1}$). This suggests that PDIF-CN2 single-fiber OPTs are a promising candidate to achieve high light responsivity in electronic devices while keeping high electron mobility.

The transfer characteristics of multifiber OPTs devices obtained at V_{DS} = +60 V in dark and under white light illumination are compared in **Figure 7 (a,b)**. In the both cases the devices were prepared in the same way using the HMDS treatment of SiO_2, the only difference being the channel length, L = 10 μm and 2.5 μm for (a) and (b), respectively. The light responsivity (R) and photocurrent/dark-current ratio (P) were calculated employing the transfer curves presented in **Figure 7a** and **7b** and their values are reported in the same figure (panels **7c** and **7d**). The channel length dependence of R and P parameters is of particular interest, because it permits a better understanding of the factors contributing to the PDI device photoresponse.

Figure 7 (a, b) shows the transfer characteristic curves of OPTs with channel lengths of 10 μm. It reveals the largest enhancement in the drain current (I_{DS}) under light irradiation due to the larger absorption of incoming photons and exhibited a photoswitching ratio P = 180. These value is 20-fold greater than the one detected in device with the shorter channel length of L = 2.5 μm (P = 9) (see **Figure 7c** and **7d**). On the other hand, the photoresponsivity R is one order of magnitude greater in the OPT devices with L = 2.5 μm. Based on these results and others obtained on thin-film devices revealing a similar behavior, we conclude that the photoswitching ratio P is independent from the channel length of PDIF-CN2 based devices, but it is dependent upon the incident optical power density (see Figure S6). However, the photoresponsivity R is strongly dependent on the channel length for both multifiber- and thin-film OPTs.

Figure S7 shows the difference in drain current in dark vs. white light irradiation for multifiber and thin-film devices measured in dry nitrogen (inside the glovebox) and in a controlled ambient air (T = 22 °C, RH ~25%). It reveals an increase in drain current upon light irradiation for multifiber-based devices by almost one order of magnitude, whereas a slight increase in drain current was observed for thin film-based OFET in a few devices while for the others a decrease in drain current were observed in dark and under white light irradiation, as a result of the semiconductor layer instability in air environment. The **Table S2** in supporting information shows different mobility and threshold voltage values extracted from the saturation regime of FET devices measured in dry nitrogen and ambient air, $\Delta\mu = (\mu_{\text{dry nitrogen}} / \mu_{\text{ambient air}})$ % measures the change between the mobility values in dry nitrogen and ambient air given in percent of the mobility in dry nitrogen and $\Delta_{Vth} = V_{th\ (\text{dry nitrogen})} - V_{th(\text{ambient air})}$ which is the threshold voltage difference between dry nitrogen and ambient air.

The mobility values reported in **Table S2** reveal that FETs based on multifiber assemblies are not affected by the exposure to oxygen, as evidenced by the unchanged mobility values measured in dry nitrogen and ambient air. For spin-coated film based devices, the electron mobility measured in ambient air drops down by almost a factor of 4 compared with that of the same device measured in dry nitrogen ($\Delta\mu = 0.09$). Based on these results, we can conclude that PDIF-CN2 air stability is strongly influenced by the molecular packing and the morphology of the semiconductor films. For multifiber assemblies the devices electrical characterizations were almost stable in ambient air; such result may be explained by the presence of tight packing between PDI cores, providing a kinetic barrier to the diffusion of oxygen into the channel.[66] Piliego et al. have reported on PDIF-CN2 based devices that the decrease in mobility cannot be attributed to semiconductor chemical degradation, but to the physisorption of atmospheric

gases[67] at the material grain boundaries which will act as electron traps[68] Zschieschang et al. showed that PDIF-CN2 vapor deposited thin-films feature a mild mobility reduction from dry nitrogen to ambient air ($\Delta\mu$ = 0.97 %), which was ascribed to the electrochemical instability of the semiconductor radical anion via the following equation:

$$O_2 + 2H_2O + 4e^- \longrightarrow 4HO^-$$

The presence of both oxygen (O_2) and water (H_2O) molecules in air environment leads to the formation of HO^- groups that act as charge traps, causing a slow decrease in carrier mobility.[69] A similar observation on electron mobility degradation in ambient air was previously reported by Morpurgo et al. on PDIF-CN2 vapor-deposited single crystals[70] Concerning the threshold voltage values (see **Table S2**), a shift towards more positive values was observed in the case of multifiber-based devices. According to Kumaki et al. this positive shift is due to the water molecules which induced a deprotonation of Si-OH groups present on the dielectric surface not passivated with OTS self-assembled monolayers, forming charge traps following the reaction: $SiOH + H_2O \rightarrow SiO^- + H_3O^+$.[71] On the other hand, a negative shift was observed for FETs based on spin-coated thin films measured in ambient air, indicating an electron doping of the semiconductor layer.

Our findings, reported in **Table S3** and **S4,** correlate μ and V_{th} and their relative variation, $\Delta\mu$, and ΔV_{th}, in dark and under white light irradiation for FET devices upon 1-day exposure to air conditions for both multifiber assemblies and spin-coated films. We can notice a threshold voltage shift towards negative values upon light irradiation for both multifiber and spin-coated devices. A decrease in electron mobility was also observed between light and dark measured both under dry nitrogen ($\Delta\mu$ = 0.96) and ambient air ($\Delta\mu$ = 0.76) environment for spin-coated

based devices, whereas no difference in electron mobility for multifibers based device was monitored, thus confirming the air stable nature of packed PDIF-CN2 fibers.

4. CONCLUSIONS

In summary, we have provided evidence for the influence of the order at the supramolecular level in the semiconducting material on the performance of field-effect transistors supported on SiO_2 substrates. In particular, the comparison of single fibers with high crystallinity fabricated from solution processable method (SIP) and multifiber assemblies with spin-coated thin films revealed that the former outperform by exhibiting good reproducibility and field-effect mobilities up to 2 $cm^2s^{-1}V^{-1}$ when the SiO_2 is treated with OTS self-assembled monolayers. Such outstanding field-effect mobility can be ascribed to intermolecular close packing arrangement within the crystalline fibers, the absence of grain boundaries and the presence of an ordered fluorocarbon layer at the periphery of the edge-on molecules ensuring the isolation of the aromatic cores from the dielectric substrate, thereby reducing the dipolar disorder, overall providing an almost ideal situation for charge transport. This mobility value is approaching those reported by Morpurgo et al. in vacuum vapor deposited single crystal devices with lengths of few millimeters.[70] Spin-coated films showed mobilities six orders of magnitude lower as a result of the poor order at the supramolecular level within the films. On the other hand, the multifibers showed mobilities of ca. 10^{-3} $cm^2s^{-1}V^{-1}$. Its discrepancy when compared to single fibers devices can be attributed to the necessity of charges to hop between adjacent fibers before reaching the metallic electrode.

We also showed that PDIF-CN2 based single-fiber OPTs exhibited higher responsivity R ($> 5 \times 10^3$ AW^{-1}), and photoswitching ratio P ($> 2 \times 10^3$) compared with that of thin-film based OPTs, which are to date the highest reported R and P obtained from PDI single crystal OPTs. This result provides evidence that also the device photoresponse depends on the molecular order and an efficient transport of the photogenerated carriers towards the electrodes is a requirement towards high light response. Overall, our SIP processed PDIF-CN2 single fibers do not require any vapor growth and are highly conducting as well as photosensitive architectures for fundamental studies on light-matter interaction and for applications in high performance opto-electronic devices.

Multifiber-based FET

devices treatment	V_{th} (V)	μ ($cm^2V^{-1}s^{-1}$)
Non-treated SiO_2	*38 ± 6*	$(4.3 \pm 0.1) \times 10^{-6}$
UV-Ozone cleaning	*30 ± 9*	$(1.1 \pm 0.1) \times 10^{-3}$
UV-Ozone/Thiol	*35 ± 5*	$(1.2 \pm 0.3) \times 10^{-3}$
HMDS SAMs	*-14 ± 4*	$(2.7 \pm 0.9) \times 10^{-3}$
HMDS/Thiol SAMs	*-15 ± 2*	$(3.0 \pm 0.7) \times 10^{-3}$
OTS SAMs	-12 ± 4	$(2.5 \pm 0.4) \times 10^{-3}$
OTS/Thiol SAMs	-18 ± 6	$(3.4 \pm 0.5) \times 10^{-3}$

Table 1. Summary of multifiber-based FET parameters measured in saturation regime. [W = 10 mm, L = 2.5 μm].

Single-fiber FET

	V_{th} (V)	μ ($cm^2V^{-1}s^{-1}$)
OTS SAMs	-10 ± 3	0.91 ± 0.04

Table 2. Summary of single-fiber top-contact bottom-gate FET parameters measured in saturation regime. [Number of samples > 10].

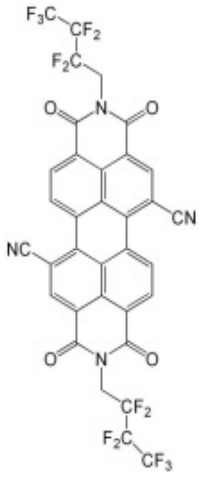

Figure 1. Chemical structure of the organic semiconductor PDIF-CN2

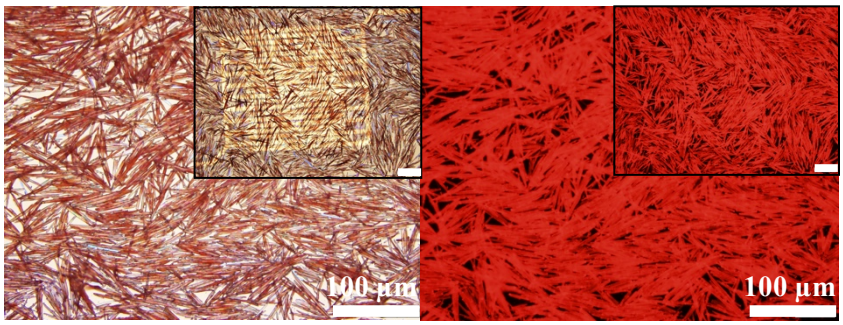

(a) **(b)**

Figure 2. Bright field **(a)** and fluorescent **(b)** optical microscopy images of SIP fibers deposited on OTS treated SiO_2. Insets: Zoom out.

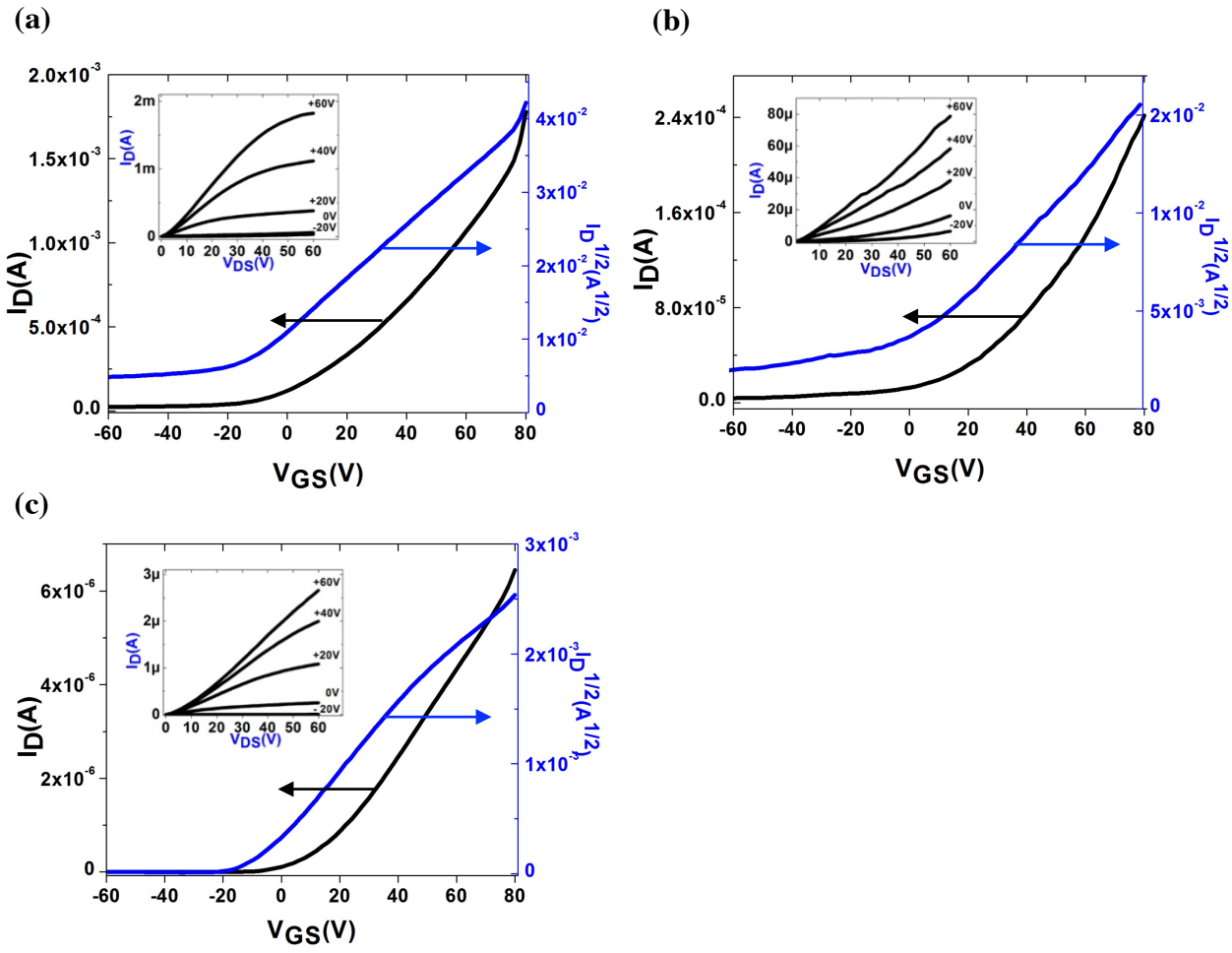

Figure 3. Transfer characteristics at V_{DS} = 60 V of PDIF-CN2 treated with OTS based on **(a)** spin-coated thin-film (L = 5 μm and W = 10 mm), **(b)** multifiber assembly (L = 5 μm and W = 10 mm), and **(c)** single fiber (L = 14 μm and W = 1.4 μm). Insets: output characteristics of each device type.

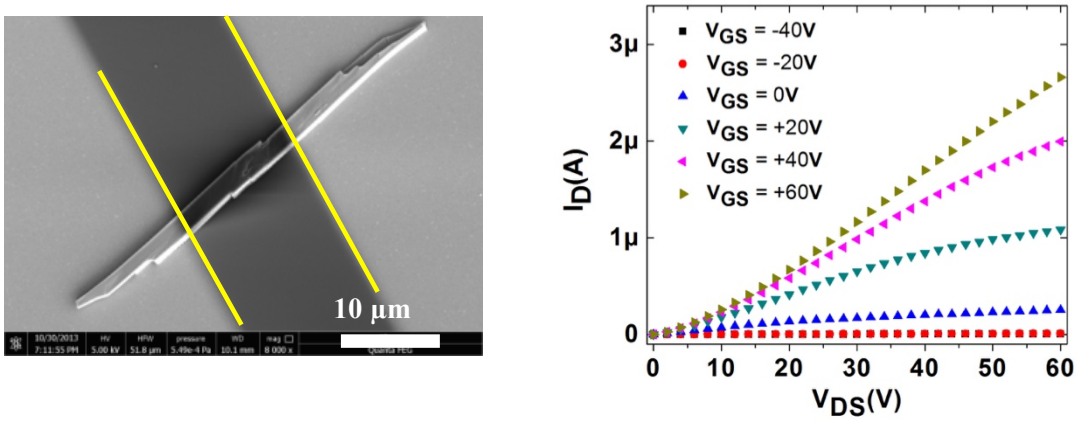

(a) **(b)**

Figure 4. SEM image **(a)** and output characteristic **(b)** of OTS treated device based on single fiber. The yellow lines in the SEM images serve as a guide to the eyes and indicate the source and drain electrode edges. (L = 14 μm and W = 1.2 μm measured from SEM image).

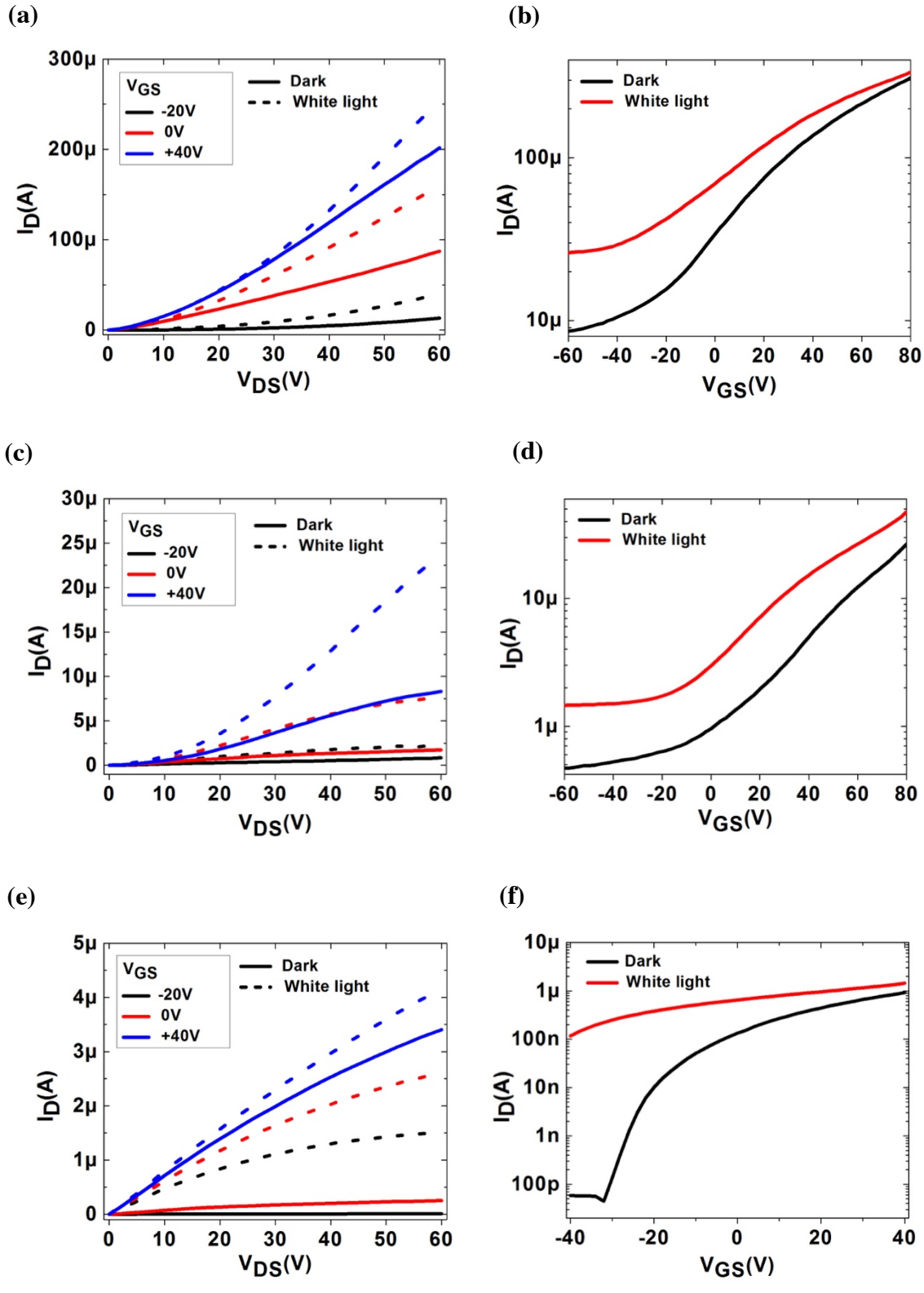
(a)
300µ
200µ
100µ
0
I_D(A)
V_{GS}
-20V
0V
+40V
Dark
White light
0
10
20
30
40
50
60
V_{DS}(V)
(b)
Dark
White light
100µ
10µ
I_D(A)
-60
-40
-20
0
20
40
60
80
V_{GS}(V)
(c)
30µ
25µ
20µ
15µ
10µ
5µ
0
I_D(A)
V_{GS}
-20V
0V
+40V
Dark
White light
0
10
20
30
40
50
60
V_{DS}(V)
(d)
Dark
White light
10µ
1µ
I_D(A)
-60
-40
-20
0
20
40
60
80
V_{GS}(V)
(e)
5µ
4µ
3µ
2µ
1µ
0
I_D(A)
V_{GS}
-20V
0V
+40V
Dark
White light
0
10
20
30
40
50
60
V_{DS}(V)
(f)
10µ
1µ
100n
10n
1n
100p
I_D(A)
Dark
White light
-40
-20
0
20
40
V_{GS}(V)

Figure 5. Comparison of **(a,c,e)** output and **(b,d,f)** transfer characteristics at V_{DS} = 60 V for **(a,b)** multi-fiber OPT, **(c,d)** thin-film OPT, and **(e,f)** single-fiber OPT measured in dark and under white light irradiation. Channel length (a-d) L= 10 μm, (e-f) L = 14 μm. $E_{white\ light}$ = 5.06 mWcm^{-2}.

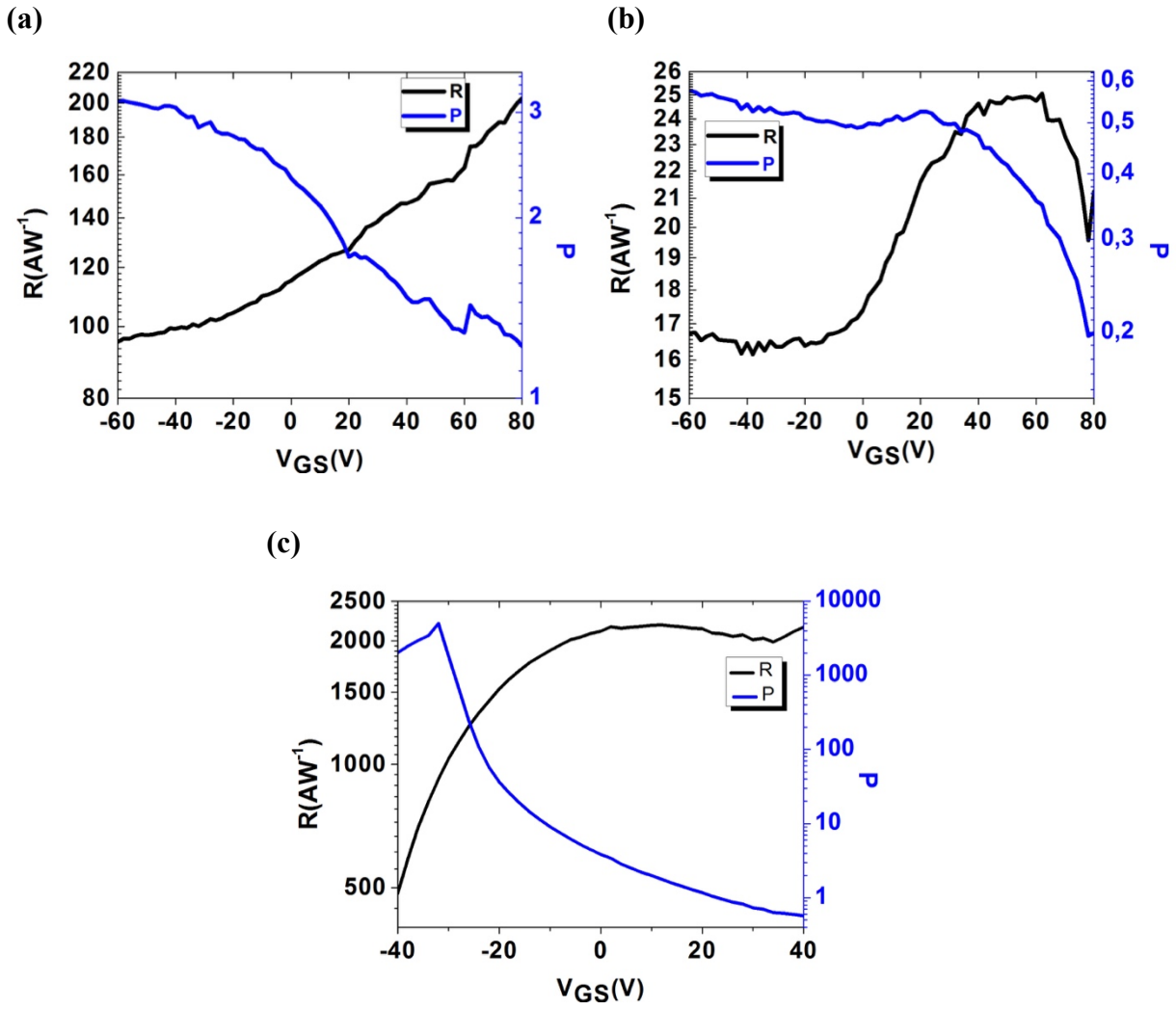

Figure 6. Variation of responsivity (R) and photosensitivity (P) with V_G at V_D = 60 V for **(a)** multifiber OPT (L = 2.5 μm), **(b)** thin-film OPT (L = 2.5 μm), and **(c)** single-fiber OPT (L = 14 μm) under white light irradiation, for devices treated with OTS. $E_{white\ light}$ = 5.06 mWcm^{-2}.

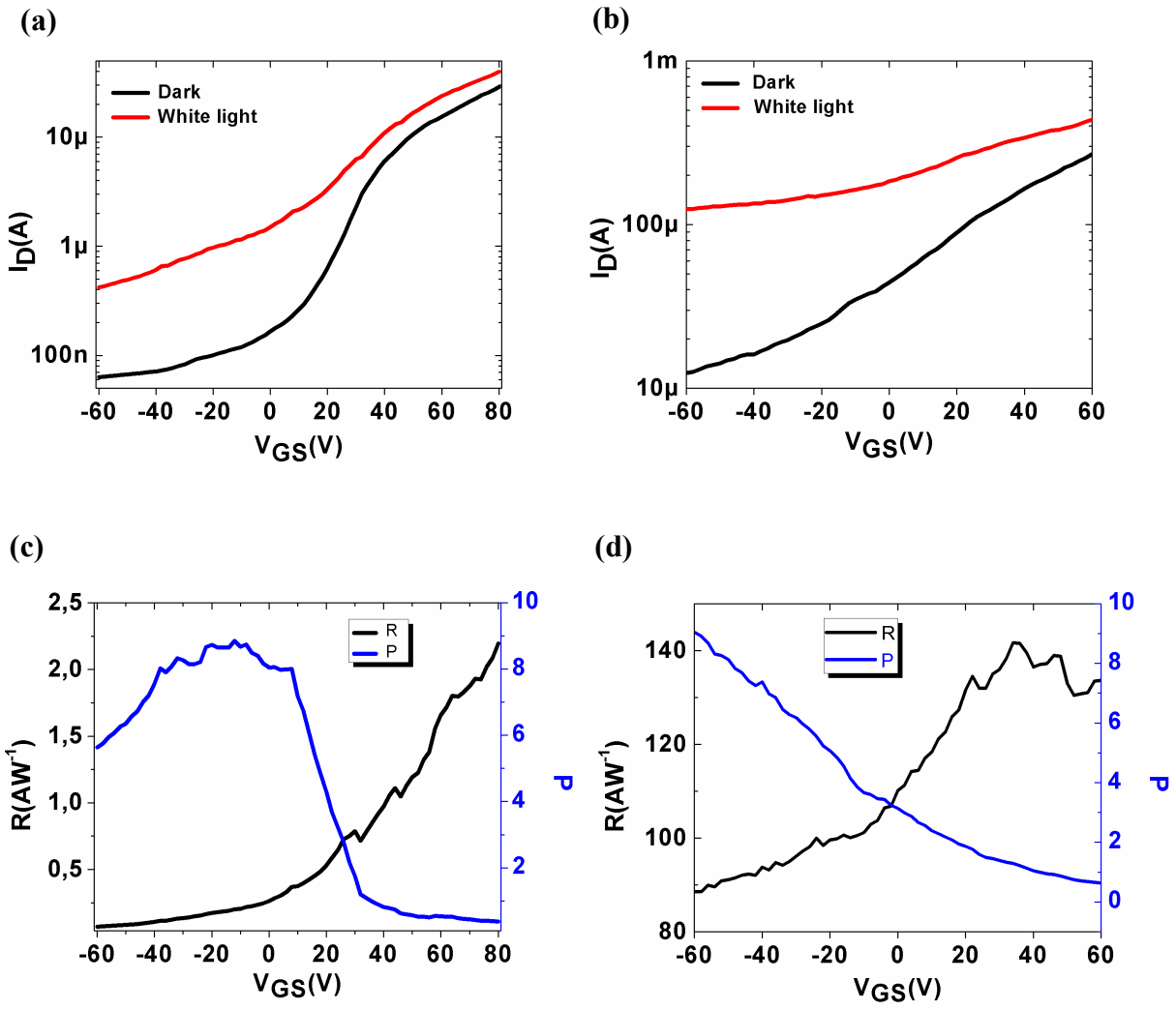

Figure 7. Transfer characteristics of multifiber OPT devices in dark and under white light irradiation treated with HMDS with different channel length **(a)** L = 10 μm and **(b)** L = 2.5 μm, and their responsivity (R) and photosensitivity, P, with V_{GS} at V_{DS} = +60 V for **(c)** L = 10 μm and **(d)** L = 2.5 μm. $E_{white\ light}$ = 5.06 mWcm^{-2}.

ASSOCIATED CONTENT

Supporting Information

Additional results, including electrical characterization obtained from the extraction of the major device parameters, Atomic Force Microscopy and Optical Microscopy characterizations of the fibers as well as optical absorption spectra in solution and Scanning Electron Microscopy were performed in order to provide a complete morphological and energetical overview of this molecular system. This material is available free of charge via the Internet at http://pubs.acs.org.

AUTHOR INFORMATION

Corresponding Author

* E-mail: samori@unistra.fr ; orgiu@unistra.fr

ACKNOWLEDGMENT

This work was financially supported by EC through the ERC project SUPRAFUNCTION (GA-257305) and the Marie Curie ITN project iSwitch (GA No. 642196), the Agence Nationale de la Recherche through the LabEx CSC (ANR-10-LABX-0026_CSC) and the International Center for Frontier Research in Chemistry (icFRC).

REFRENCES

1. Dimitrakopoulos, C. D.; Malenfant, P. R. L., Organic Thin Film Transistors for Large Area Electronics. *Adv. Mater.* **2002,** *14* (2), 99-117.
2. Tian, H. K.; Shi, J. W.; Yan, D. H.; Wang, L. X.; Geng, Y. H.; Wang, F. S., Naphthyl end-Capped Quarterthiophene: A Simple Organic Semiconductor with High Mobility and Air Stability. *Adv. Mater.* **2006,** *18* (16), 2149-2152.

3. Facchetti, A., Semiconductors for Organic Transistors. *Mater. Today* **2007,** *10* (3), 28-37.
4. Zaumseil, J.; Sirringhaus, H., Electron and Ambipolar Transport in Organic Field-Effect Transistors. *Chem. Rev.* **2007,** *107* (4), 1296-1323.
5. Murphy, A. R.; Fréchet, J. M. J., Organic Semiconducting Oligomers for Use in Thin Film Transistors. *Chem. Rev.* **2007,** *107* (4), 1066-1096.
6. Mas-Torrent, M.; Rovira, C., Novel Small Molecules for Organic Field-Effect Transistors: Towards Processability and High Performance. *Chem. Soc. Rev.* **2008,** *37* (4), 827-838.
7. Würthner, F.; Stolte, M., Naphthalene and Perylene Diimides for Organic Transistors. *Chem. Commun.* **2011,** *47* (18), 5109-5115.
8. Klauk, H.; Halik, M.; Zschieschang, U.; Schmid, G.; Radlik, W.; Weber, W., High-Mobility Polymer Gate Dielectric Pentacene Thin Film Transistors. *J. Appl. Phys.* **2002,** *92* (9), 5259-5263.
9. Torsi, L.; Farinola, G. M.; Marinelli, F.; Tanese, M. C.; Omar, O. H.; Valli, L.; Babudri, F.; Palmisano, F.; Zambonin, P. G.; Naso, F., A Sensitivity-Enhanced Field-Effect Chiral Sensor. *Nat Mater* **2008,** *7* (5), 412-417.
10. Caboni, A.; Orgiu, E.; Barbaro, M.; Bonfiglio, A., Flexible Organic Thin-Film Transistors for pH Monitoring. *IEEE Sens J* **2009,** *9* (12), 1963-1970.
11. Caboni, A.; Orgiu, E.; Scavetta, E.; Barbaro, M.; Bonfiglio, A., Organic-Based Sensor for Chemical Detection in Aqueous Solution. *Appl Phys Lett* **2009,** *95* (12), 123304.
12. Gao, X. K.; Di, C. A.; Hu, Y. B.; Yang, X. D.; Fan, H. Y.; Zhang, F.; Liu, Y. Q.; Li, H. X.; Zhu, D. B., Core-Expanded Naphthalene Diimides Fused with 2-(1,3-Dithiol-2-Ylidene)Malonitrile Groups for High-Performance, Ambient-Stable, Solution-Processed n-Channel Organic Thin Film Transistors. *J. Am. Chem. Soc.* **2010,** *132* (11), 3697-3699.
13. Angione, M. D.; Cotrone, S.; Magliulo, M.; Mallardi, A.; Altamura, D.; Giannini, C.; Cioffi, N.; Sabbatini, L.; Fratini, E.; Baglioni, P.; Scamarcio, G.; Palazzo, G.; Torsi, L., Interfacial Electronic Effects in Functional Biolayers Integrated into Organic Field-Effect Transistors. *Proc. Natl. Acad. Sci. U.S.A.* **2012,** *109* (17), 6429-6434.
14. Palazzo, G.; Magliulo, M.; Mallardi, A.; Angione, M. D.; Gobeljic, D.; Scamarcio, G.; Fratini, E.; Ridi, F.; Torsi, L., Electronic Transduction of Proton Translocations in Nanoassembled Lamellae of Bacteriorhodopsin. *Acs Nano* **2014,** *8* (8), 7834-7845.
15. Arias, A. C.; MacKenzie, J. D.; McCulloch, I.; Rivnay, J.; Salleo, A., Materials and Applications for Large Area Electronics: Solution-Based Approaches. *Chem. Rev.* **2010,** *110* (1), 3-24.
16. Olivier, Y.; Niedzialek, D.; Lemaur, V.; Pisula, W.; Müllen, K.; Koldemir, U.; Reynolds, J. R.; Lazzaroni, R.; Cornil, J.; Beljonne, D., 25th Anniversary Article: High-Mobility Hole and Electron Transport Conjugated Polymers: How Structure Defines Function. *Adv. Mater.* **2014,** *26* (14), 2119-2136.
17. Burroughes, J. H.; Bradley, D. D. C.; Brown, A. R.; Marks, R. N.; Mackay, K.; Friend, R. H.; Burn, P. L.; Holmes, A. B., Light-Emitting-Diodes Based on Conjugated Polymers. *Nature* **1990,** *347* (6293), 539-541.
18. Greenham, N. C.; Moratti, S. C.; Bradley, D. D. C.; Friend, R. H.; Holmes, A. B., Efficient Light-Emitting-Diodes Based on Polymers with High Electron-Affinities. *Nature* **1993,** *365* (6447), 628-630.

19. Brabec, C. J.; Cravino, A.; Meissner, D.; Sariciftci, N. S.; Fromherz, T.; Rispens, M. T.; Sanchez, L.; Hummelen, J. C., Origin of the Open Circuit Voltage of Plastic Solar Cells. *Adv. Funct. Mater.* **2001,** *11* (5), 374-380.
20. Cavallini, M.; Gentili, D.; Greco, P.; Valle, F.; Biscarini, F., Micro- and Nanopatterning by Lithographically Controlled Wetting. *Nat. Protoc.* **2012,** *7* (9), 1668-1676.
21. Cavallini, M.; D'Angelo, P.; Criado, V. V.; Gentili, D.; Shehu, A.; Leonardi, F.; Milita, S.; Liscio, F.; Biscarini, F., Ambipolar Multi-Stripe Organic Field-Effect Transistors. *Adv. Mater.* **2011,** *23* (43), 5091-5097.
22. Qi, Z.; Liao, X. X.; Zheng, J. C.; Di, C. A.; Gao, X. K.; Wang, J. Z., High-Performance n-Type Organic Thin-Film Phototransistors Based on a Core-Expanded Naphthalene Diimide. *Appl Phys Lett* **2013,** *103* (5), 053301.
23. Guo, N.; Hu, W. D.; Liao, L.; Yip, S.; Ho, J. C.; Miao, J. S.; Zhang, Z.; Zou, J.; Jiang, T.; Wu, S. W.; Chen, X. S.; Lu, W., Anomalous and Highly Efficient InAs Nanowire Phototransistors Based on Majority Carrier Transport at Room Temperature. *Adv. Mater.* **2014,** *26* (48), 8203-8209.
24. Kim, J.; Cho, S.; Kim, Y. H.; Park, S. K., Highly-Sensitive Solution-Processed 2,8-difluoro-5,11-bis(triethylsilylethynyl) Anthradithiophene (diF-TESADT) Phototransistors for Optical Sensing Applications. *Org. Electron.* **2014,** *15* (9), 2099-2106.
25. Kim, M.; Ha, H. J.; Yun, H. J.; You, I. K.; Baeg, K. J.; Kim, Y. H.; Ju, B. K., Flexible Organic Phototransistors Based on a Combination of Printing Methods. *Org. Electron.* **2014,** *15* (11), 2677-2684.
26. Loffredo, F.; Bruno, A.; Del Mauro, A. D.; Grimaldi, I. A.; Miscioscia, R.; Nenna, G.; Pandolfi, G.; Petrosino, M.; Villani, F.; Minarini, C.; Facchetti, A., Photoresponse of Pentacene-Based Transistors. *Phys. Status Solidi A* **2014,** *211* (2), 460-466.
27. Yang, D.; Zhang, L.; Wang, H. W.; Wang, Y. S.; Li, Z. X.; Song, T. J.; Fu, C. J.; Yang, S. Y.; Zou, B. S., Pentacene-Based Photodetector in Visible Region With Vertical Field-Effect Transistor Configuration. *IEEE Photonics Technol. Lett.* **2015,** *27* (3), 233-236.
28. Li, M. M.; An, C. B.; Marszalek, T.; Guo, X.; Long, Y. Z.; Yin, H. X.; Gu, C. Z.; Baumgarten, M.; Pisula, W.; Müllen, K., Phenanthrene Condensed Thiadiazoloquinoxaline Donor-Acceptor Polymer for Phototransistor Applications. *Chem. Mat.* **2015,** *27* (6), 2218-2223.
29. Ljubic, D.; Smithson, C. S.; Wu, Y. L.; Zhu, S. P., Highly UV-Sensitive and Responsive Benzothiophene/Dielectric Polymer Blend-Based Organic Thin-Film Phototransistor. *Adv. Electron. Mater.* **2015,** *1* (8), 1500119.
30. Di Maria, F.; Olivelli, P.; Gazzano, M.; Zanelli, A.; Biasiucci, M.; Gigli, G.; Gentili, D.; D'Angelo, P.; Cavallini, M.; Barbarella, G., A Successful Chemical Strategy To Induce Oligothiophene Self-Assembly into Fibers with Tunable Shape and Function. *J. Am. Chem. Soc.* **2011,** *133* (22), 8654-8661.
31. Gentili, D.; Di Maria, F.; Liscio, F.; Ferlauto, L.; Leonardi, F.; Maini, L.; Gazzano, M.; Milita, S.; Barbarella, G.; Cavallini, M., Targeting Ordered Oligothiophene Fibers with Enhanced Functional Properties by Interplay of Self-Assembly and Wet Lithography. *J. Mater. Chem.* **2012,** *22* (39), 20852-20856.
32. Kim, K. H.; Bae, S. Y.; Kim, Y. S.; Hur, J. A.; Hoang, M. H.; Lee, T. W.; Cho, M. J.; Kim, Y.; Kim, M.; Jin, J. I.; Kim, S. J.; Lee, K.; Lee, S. J.; Choi, D. H., Highly Photosensitive J-Aggregated Single-Crystalline Organic Transistors. *Adv. Mater.* **2011,** *23* (27), 3095-3099.

33. Liu, X. H.; Tavares, L.; Osadnik, A.; Lausen, J. L.; Kongsted, J.; Lutzen, A.; Rubahn, H. G.; Kjelstrup-Hansen, J., Low-Voltage Organic Phototransistors Based on Naphthyl end-Capped Oligothiophene Nanofibers. *Org. Electron.* **2014,** *15* (6), 1273-1281.
34. Um, H. A.; Lee, D. H.; Heo, D. U.; Yang, D. S.; Shin, J.; Baik, H.; Cho, M. J.; Choi, D. H., High Aspect Ratio Conjugated Polymer Nanowires for High Performance Field-Effect Transistors and Phototransistors. *ACS Nano* **2015,** *9* (5), 5264-5274.
35. Zhao, G. Y.; Liu, J.; Meng, Q.; Ji, D. Y.; Zhang, X. T.; Zou, Y.; Zhen, Y. G.; Dong, H. L.; Hu, W. P., High-Performance UV-Sensitive Organic Phototransistors Based on Benzo 1,2-b:4,5-b ' dithiophene Dimers Linked with Unsaturated Bonds. *Adv. Electron. Mater.* **2015,** *1* (8), 1500071.
36. Wu, G.; Chen, C.; Liu, S.; Fan, C. C.; Li, H. Y.; Chen, H. Z., Solution-Grown Organic Single-Crystal Field-Effect Transistors with Ultrahigh Response to Visible-Blind and Deep UV Signals. *Adv. Electron. Mater.* **2015,** *1* (8), 1500136.
37. Guan, Y. S.; Qin, Y. K.; Sun, Y. H.; Wang, C.; Xu, W.; Zhu, D. B., Single-Bundle Nanofiber Based OFETs Fabricated from a Cyclic Conjugated Organogelator with High Field-Effect Mobility and High Photoresponsivity. *Chem. Commun.* **2015,** *51* (61), 12182-12184.
38. Wang, J. Y.; Peng, H. D.; Yang, J. M.; Yan, J. H.; Pan, G. B., Solvent-Induced Self-Assembly Synthesis of Ultralong Single Crystalline Organic NiOEP Nanowires with High Photoconductivity. *RSC Adv.* **2015,** *5* (91), 74251-74255.
39. Guo, Y. L.; Du, C. Y.; Yu, G.; Di, C. A.; Jiang, S. D.; Xi, H. X.; Zheng, J.; Yan, S. K.; Yu, C. L.; Hu, W. P.; Liu, Y. Q., High-Performance Phototransistors Based on Organic Microribbons Prepared by a Solution Self-Assembly Process. *Adv. Funct. Mater.* **2010,** *20* (6), 1019-1024.
40. Zhang, Y. T.; Song, X. X.; Wang, R.; Cao, M. X.; Wang, H. Y.; Che, Y. L.; Ding, X.; Yao, J. Q., Comparison of Photoresponse of Transistors Based on Graphene-Quantum Dot Hybrids with Layered and Bulk Heterojunctions. *Nanotechnology* **2015,** *26* (33), 335201-335208.
41. Song, X. X.; Zhang, Y. T.; Wang, R.; Cao, M. X.; Che, Y. L.; Wang, J. L.; Wang, H. Y.; Jin, L. F.; Dai, H. T.; Ding, X.; Zhang, G. Z.; Yao, J. Q., Bulk- and Layer-Heterojunction Phototransistors Based on Poly 2-methoxy-5-(2 '-ethylhexyloxy-p-phenylenevinylene) and PbS Quantum Dot Hybrids. *Appl Phys Lett* **2015,** *106* (25), 253501.
42. Nollau, A.; Hoffmann, M.; Fritz, T.; Leo, K., Dissociation of Excitons in Organic Dye Layers of Perylene Derivatives. *Thin Solid Films* **2000,** *368* (1), 130-137.
43. Chesterfield, R. J.; McKeen, J. C.; Newman, C. R.; Ewbank, P. C.; da Silva, D. A.; Bredas, J. L.; Miller, L. L.; Mann, K. R.; Frisbie, C. D., Organic Thin Film Transistors Based on N-Alkyl Perylene Diimides: Charge Transport Kinetics as a Function of Gate Voltage and Temperature. *J. Phys. Chem. B* **2004,** *108* (50), 19281-19292.
44. Sergeyev, S.; Pisula, W.; Geerts, Y. H., Discotic Liquid Crystals: A New Generation of Organic Semiconductors. *Chem. Soc. Rev.* **2007,** *36* (12), 1902-1929.
45. Feng, Y.; Feng, W., Photo-Responsive Perylene Diimid–Azobenzene Dyad: Photochemistry and its Morphology Control by Self-Assembly. *Opt Mater* **2008,** *30* (6), 876-880.
46. Schmidt, R.; Oh, J. H.; Sun, Y.-S.; Deppisch, M.; Krause, A.-M.; Radacki, K.; Braunschweig, H.; Koenemann, M.; Erk, P.; Bao, Z.; Würthner, F., High-Performance Air-Stable n-Channel Organic Thin Film Transistors Based on Halogenated Perylene Bisimide Semiconductors. *J. Am. Chem. Soc* **2009,** *131* (17), 6215-6228.
47. Anthony, J. E.; Facchetti, A.; Heeney, M.; Marder, S. R.; Zhan, X. W., n-Type Organic Semiconductors in Organic Electronics. *Adv. Mater.* **2010,** *22* (34), 3876-3892.

48. El Gemayel, M.; Treier, M.; Musumeci, C.; Li, C.; Müllen, K.; Samorì, P., Tuning the Photoresponse in Organic Field-Effect Transistors. *J. Am. Chem. Soc.* **2012,** *134* (4), 2429-2433.
49. Mukherjee, B.; Sim, K.; Shin, T. J.; Lee, J.; Mukherjee, M.; Ree, M.; Pyo, S., Organic Phototransistors Based on Solution Grown, Ordered Single Crystalline Arrays of a pi-Conjugated Molecule. *J. Mater. Chem.* **2012,** *22* (7), 3192-3200.
50. Yu, H.; Bao, Z. A.; Oh, J. H., High-Performance Phototransistors Based on Single-Crystalline n-Channel Organic Nanowires and Photogenerated Charge-Carrier Behaviors. *Adv. Funct. Mater.* **2013,** *23* (5), 629-639.
51. Pfattner, R.; Pavlica, E.; Jaggi, M.; Liu, S. X.; Decurtins, S.; Bratina, G.; Veciana, J.; Mas-Torrent, M.; Rovira, C., Photo-Induced Intramolecular Charge Transfer in an Ambipolar Field-Effect Transistor Based on a pi-Conjugated Donor-Acceptor Dyad. *J Mater Chem C* **2013,** *1* (25), 3985-3988.
52. Tozlu, C.; Kus, M.; Can, M.; Ersöz, M., Solution Processed White Light Photodetector Based N, N '-di(2-ethylhexyl)-3,4,9,10-perylene Diimide Thin Film Phototransistor. *Thin Solid Films* **2014,** *569*, 22-27.
53. Yu, H.; Joo, P.; Lee, D.; Kim, B.-S.; Oh, J. H., Photoinduced Charge-Carrier Dynamics of Phototransistors Based on Perylene Diimide/Reduced Graphene Oxide Core/Shell p-n Junction Nanowires. *Adv. Opt. Mater.* **2015,** *3* (2), 241-247.
54. Mativetsky, J. M.; Orgiu, E.; Lieberwirth, I.; Pisula, W.; Samorì, P., Charge Transport Over Multiple Length Scales in Supramolecular Fiber Transistors: Single Fiber Versus Ensemble Performance. *Adv. Mater.* **2014,** *26* (3), 430-435.
55. Jones, B. A.; Ahrens, M. J.; Yoon, M. H.; Facchetti, A.; Marks, T. J.; Wasielewski, M. R., High-Mobility Air-Stable n-Type Semiconductors with Processing Versatility: Dicyanoperylene-3,4 : 9,10-bis(dicarboximides). *Angew. Chem., Int. Ed.* **2004,** *43* (46), 6363-6366.
56. Schmidt, R.; Ling, M. M.; Oh, J. H.; Winkler, M.; Konemann, M.; Bao, Z. N.; Wurthner, F., Core-Fluorinated Rerylene Bisimide Dyes: Air Stable n-Channel Organic Semiconductors for Thin Film Transistors with Exceptionally High On-to-Off Current Ratios. *Adv. Mater.* **2007,** *19* (21), 3692-3695.
57. Jones, B. A.; Facchetti, A.; Wasielewski, M. R.; Marks, T. J., Effects of Arylene Diimide Thin Film Growth Conditions on n-Channel OFET Performance. *Adv. Funct. Mater.* **2008,** *18* (8), 1329-1339.
58. Fabiano, S.; Wang, H.; Piliego, C.; Jaye, C.; Fischer, D. A.; Chen, Z. H.; Pignataro, B.; Facchetti, A.; Loo, Y. L.; Loi, M. A., Supramolecular Order of Solution-Processed Perylenediimide Thin Films: High-Performance Small-Channel n-Type Organic Transistors. *Adv. Funct. Mater.* **2011,** *21* (23), 4479-4486.
59. Minder, N. A.; Ono, S.; Chen, Z. H.; Facchetti, A.; Morpurgo, A. F., Band-Like Electron Transport in Organic Transistors and Implication of the Molecular Structure for Performance Optimization. *Adv. Mater.* **2012,** *24* (4), 503-508.
60. Willa, K.; Hausermann, R.; Mathis, T.; Facchetti, A.; Chen, Z.; Batlogg, B., From Organic Single Crystals to Solution Processed Thin-Films: Charge Transport and Trapping with Varying Degree of Order. *J. Appl. Phys.* **2013,** *113* (13).
61. de Boer, B.; Hadipour, A.; Mandoc, M. M.; van Woudenbergh, T.; Blom, P. W. M., Tuning of Metal Work Functions with Self-Assembled Monolayers. *Adv. Mater.* **2005,** *17* (5), 621-625.

62. Chua, L. L.; Zaumseil, J.; Chang, J. F.; Ou, E. C. W.; Ho, P. K. H.; Sirringhaus, H.; Friend, R. H., General Observation of n-Type Field-Effect Behaviour in Organic Semiconductors. *Nature* **2005,** *434* (7030), 194-199.
63. Cramer, T.; Kyndiah, A.; Kloes, A.; Murgia, M.; Fraboni, B.; Biscarini, F., Charge Density Increase in Submonolayer Organic Field-Effect Transistors. *Phys. Rev. B* **2015,** *91* (20), 205305-205305-7.
64. Beljonne, D.; Pourtois, G.; Silva, C.; Hennebicq, E.; Herz, L. M.; Friend, R. H.; Scholes, G. D.; Setayesh, S.; Müllen, K.; Brédas, J. L., Interchain vs. Intrachain Energy Transfer in Acceptor-Capped Conjugated Polymers. *Proc. Natl. Acad. Sci. U.S.A.* **2002,** *99* (17), 10982-10987.
65. Mollay, B.; Lemmer, U.; Kersting, R.; Mahrt, R. F.; Kurz, H.; Kauffman, H. F.; Bässler, H., Dynamics of Singlet Excitations in Conjugated Polymers - Poly (PhenyleneVinylene) and Poly (PhenylPhenyleneVinylene). *Phys. Rev. B* **1994,** *50* (15), 10769-10779.
66. Weitz, R. T.; Amsharov, K.; Zschieschang, U.; Villas, E. B.; Goswami, D. K.; Burghard, M.; Dosch, H.; Jansen, M.; Kern, K.; Klauk, H., Organic n-Channel Transistors Based on Core-Cyanated Perylene Carboxylic Diimide Derivatives. *J. Am. Chem. Soc.* **2008,** *130* (14), 4637-4645.
67. Jones, B. A.; Facchetti, A.; Wasielewski, M. R.; Marks, T. J., Tuning Orbital Energetics in Arylene Diimide Semiconductors. Materials Design for Ambient Stability of n-Type Charge Transport. *J. Am. Chem. Soc.* **2007,** *129* (49), 15259-15278.
68. Piliego, C.; Jarzab, D.; Gigli, G.; Chen, Z. H.; Facchetti, A.; Loi, M. A., High Electron Mobility and Ambient Stability in Solution-Processed Perylene-Based Organic Field-Effect Transistors. *Adv. Mater.* **2009,** *21* (16), 1573-1576
69. Zschieschang, U.; Amsharov, K.; Jansen, M.; Kern, K.; Klauk, H.; Weitz, R. T., Separating the Impact of Oxygen and Water on the Long-Term Stability of n-Channel Perylene Diimide Thin-Film Transistors. *Org. Electron.* **2015,** *26*, 340-344.
70. Molinari, A. S.; Alves, H.; Chen, Z.; Facchetti, A.; Morpurgo, A. F., High Electron Mobility in Vacuum and Ambient for PDIF-CN2 Single-Crystal Transistors. *J. Am. Chem. Soc.* **2009,** *131* (7), 2462-2463.
71. Kumaki, D.; Umeda, T.; Tokito, S., Influence of H2O and O2 on Threshold Voltage Shift in Organic Thin-Film Transistors: Deprotonation of SiOH on SiO2 Gate-Insulator Surface. *Appl Phys Lett* **2008**, *92* (9), 093309.